Highlights

Improving Energy Flexibility and PV Self-Consumption for a Tropical Net Zero Energy Office Building

Sicheng Zhan,Bing Dong,Adrian Chong

- Enhanced energy flexibility and PV local consumption via MPC in actual offices.
- PV self-consumption and building self-sufficiency improved by 19.5% and 10.6%.
- Evaluated different levels of data availability under various control scenarios.
- Weather conditions had a stronger impact on control than other tested data points.
- Proposed a data-centric control framework for improved scalability and robustness.

Cite as: Zhan, S., Dong, B., & Chong, A. (2023). Improving energy flexibility and PV self-consumption for a tropical net zero energy office building. Energy and Buildings, 278, 112606.
doi: https://doi.org/10.1016/j.enbuild.2022.112606

Improving Energy Flexibility and PV Self-Consumption for a Tropical Net Zero Energy Office Building

Sicheng Zhan[a], Bing Dong[b] and Adrian Chong[a,*]

[a]Department of the Built Environment, National University of Singapore, 117566, Singapore
[b]Department of Mechanical & Aerospace Engineering, Syracuse University, NY 13244, USA

ARTICLE INFO

Keywords:
Energy flexibility
Self-consumption
Self-sufficiency
Data-centric MPC
Net zero energy building
Model predictive control

ABSTRACT

Building energy flexibility is crucial for improving the local consumption of renewable energy and enhancing building self-sufficiency. The abundant solar energy resource in the tropics presents a great opportunity to reduce carbon emission and achieve net-zero, but the building energy flexibility remains understudied in the region. Hence, this study proposed and implemented a practical control framework based on Model Predictive Control (MPC) that uncovers the energy flexibility potential of a tropical office building with hybrid cooling systems. Considering the impact of data availability on the actual control performance, MPC with alternative data usage configurations were also investigated in actual and virtual end-to-end experiments. It was first demonstrated that the proposed framework effectively regulated the building load. Compared with the baseline control, the PV self-consumption and the building self-sufficiency were respectively improved by 19.5% and 10.6%. Among the three data categories tested (internal disturbance, external disturbance, and system condition), accurate local weather conditions were shown to be the most critical for desirable control results. Moreover, the benefit of higher data granularity under different building characteristics was quantified in the simulation. Based on the systematic experiments, the relationships between the data availability and control performance were established. Accordingly, a data-centric framework was proposed to enhance the reproducibility and scalability of optimal control studies. Future research can be guided to facilitate large-scale real-world implementations.

1. Introduction

Renewable energy is a promising approach to mitigating climate change and addressing the arising concern of energy security [1]. Hence, the percentage of global renewable electricity generation has rapidly increased during the past decade [2], and further growth is expected given the decarbonization goals set by many countries around the world. While replacing fossil fuels and reducing carbon emissions, renewable energy resources typically observe significant uncertainty and variability, presenting power balancing and flexibility challenges to the current power grid [3]. For example, a considerable amount of renewable power that the grid cannot accommodate had to be curtailed [4]. Contributing to more than a third of global energy consumption [5], buildings are critical in tackling these challenges and therefore the focus of this study.

1.1. Solar photovoltaic self-consumption

Solar Photovoltaics (PV) is a renewable energy resource available at any scale and almost any location, whose penetration has been promoted by subsidies on its installation [6]. Since most PV installations are currently on-grid, the generated power does not have to be consumed locally. However, the fast PV penetration resulted in the generation-load mismatch and corresponding grid operating risks such as the well-known duck curve, where the fluctuating daily demand curve of the entire threatens the operations of traditional power plants [7]. Such problems could become more severe as the percentage of PV generation keeps increasing. One approach to addressing this problem is to form smart microgrids with interconnected loads and distributed PV systems that can operate both on and off the grid [8]. The self-consumption of PV power has manifold benefits, such as enhancing the grid stability with less fluctuating loads, reducing consumers' energy costs through self-sufficiency, and enabling the downsizing of traditional power plants in the longer term to facilitate renewable energy integration [9].

szhan@u.nus.edu (S. Zhan); bidong@syr.edu (B. Dong); adrian.chong@nus.edu.sg (A. Chong)
ORCID(s): 0000-0002-9872-8555 (S. Zhan); 0000-0002-9486-4728 (A. Chong)

The PV self-consumption can be improved by either shifting the generation or shifting the load [10]. Since solar power is not controllable, the generation can only be shifted through energy storage systems (ESS). Thermal ESS has been shown effective for both short-term [11], and seasonal [12] shifting. However, the application of thermal ESS requires compatible HVAC systems and desirable climate conditions [13]. In contrast, electrical ESS such as batteries have better compatibility and flexibility to shift the generation for several hours with different HVAC systems and across different climates [14, 15]. Nevertheless, current battery technologies suffer from short lifetimes and high initial investment [16]. Besides, the available electricity storage capacity is typically dozens of times smaller than the total renewable power capacity or the peak-valley load difference [17]. Therefore, in addition to ESS, load shifting through demand-side management (DSM) is critical for integrating renewable energy and reducing carbon emissions.

DSM refers to strategies or techniques to pursue grid-friendly energy consumption behaviors, such as peak clipping and valley filling [18]. The building sector, as a major consumer, is the main subject of DSM. For example, Aghajani et al. [19] applied multi-objective optimization to coordinate several energy resources and buildings on a microgrid, saved 24% of operating costs, and reduced carbon emissions by 16%. Lizana et al. [20] optimized the heat pump and latent heat storage operational strategies, leading to 20% electricity cost-savings for the end-users and 25% for the retailers. Zhang and Kummert [21] presented over 20% peak reduction through thermostat control for space heating. Apart from being a major consumer, another pillar of the buildings' vital role in DSM is their energy flexibility. Annex 67 defines the energy flexibility of a building as *"the ability to manage its demand and generation according to local climate conditions, user needs, and energy network requirements"* [22]. Noting that DSM and energy flexibility studies often involve ESS, further discussions in this paper focus on buildings' intrinsic flexibility resources given the aforementioned limitations of ESS.

1.2. Energy flexibility of tropical non-residential buildings

Building thermal mass and the usage of electrical appliances are two major intrinsic resources to provide energy flexibility. As the heat capacity of indoor air is relatively small, the thermal mass of a building mainly comprises the envelope and the internal mass. Combined with optimal HVAC control strategies, the thermal mass was utilized to reduce the demand in a short period [23]. Phase change materials can potentially be integrated into envelopes and furniture to enlarge thermal mass and strengthen energy flexibility [24]. Considering that different zones are not always occupied and that occupants accept indoor environments within certain comfort ranges, HVAC systems can serve flexibility through temperature setpoint reset and pre-conditioning. For example, over 40% of demand reduction and up to 15% of cost-savings were achieved with optimized setpoint schedules [25], and adjusting temperature setpoints could realize peak-shaving without sacrificing thermal comfort [26]. Besides, a large portion of building energy consumption is attributed to occupants' activity of using electrical appliances, especially in residential buildings [27]. Accordingly, non-essential usage of some appliances can be scheduled to fulfill demand response requests [28].

Although the national solar penetration levels in most tropical countries have yet to surge, solar energy resource is rich in tropical regions, which provides opportunities for net zero energy buildings (NZEB) in the regions [29]. While it is not intrusive to on-grid operate a small number of NZEB, the prospect of integrating a larger percentage of solar energy and NZEB desires the solar generation to be consumed on-site. Yet, little research effort has been devoted to energy flexibility for non-residential buildings in the tropics thus far [30], possibly because 1) the acceptable range of room temperature is narrower for cooling, 2) buildings typically have relatively light thermal mass in hot and humid climates [31], and 3) electrical appliances usage is likely to be essential and unshiftable in non-residential buildings. Considering that the cooling energy is highly related to the room temperature, one approach to improving the energy flexibility of tropical office buildings is to expand the acceptable temperature range. Complementing air conditioning systems with ceiling fans that elevate the air movement, referred to as hybrid cooling in the rest of this paper, provides thermal comfort with different combinations of room temperature and fan speed [32]. Since the fan speed can be easily and instantly adjusted, the acceptable temperature range becomes wider than traditional cooling. Taking this advantage, it is possible to apply advanced control strategies and exploit energy flexibility in tropical buildings.

1.3. Data requirements of realizing energy flexibility

Apart from the building systems, a robust optimal control framework is critical for realizing energy flexibility. Model predictive control (MPC), as an established control approach, has been shown effective in many studies [33]. Yet, it is still challenging to apply optimal control in actual buildings, and real-world applications remain limited [34]. One primary barrier is the heterogeneity of buildings, making existing methods hardly generalizable. Consequently, the configuration procedure is consuming and highly expert-driven. Meanwhile, it is not straightforward to inform

the control performance before implementation, which is necessary for scalable applications. Recent studies have recognized that data availability and quality are essential for downstream application performance [35, 36]. However, there is a paucity of research that systematically investigates the significance of different data streams in control applications.

Building operations have generated a large amount of data in recent years as the rapid deployment of the Internet of Things (IoT) and data acquisition systems. While fueling the research on many optimization-based applications such as MPC, these data present great challenges of data management and utilization for scalable implementations in actual buildings [34]. First, many practical issues are of concern when installing sensors, including cost, reliability, accuracy, and data management issues [37]. Therefore, acquiring a quality and cost-effective dataset is critical for applications at scale [38]. Moreover, building operations are subject to substantial uncertainties, which are difficult, if not impossible, to fully quantify. For example, most occupant behaviors are either immeasurable or unmeasured in practice, and ambient weather conditions are usually measured at low spatial resolution. Consequently, operational data is typically sparse in buildings, which affects the reliability of predictive models and control optimization. Thus, understanding the data requirements is as important as establishing the control methods [39].

1.4. Research objectives

To sum up, building energy flexibility is crucial for facilitating solar energy integration and alleviating grid reliance. Hybrid cooling systems bring tropical buildings an opportunity to enhance their energy flexibility, but a robust control method is required to realize the potential. To this end, this study provides an optimal control framework that improves the energy flexibility of tropical office buildings. There are three research objectives:

1. Propose an integrative control framework based on MPC that realizes the energy flexibility of tropical office buildings, improving PV self-consumption and building self-sufficiency.
2. Implement the proposed framework in a multi-zone office space and benchmark its performance against baseline controls in both virtual and actual experiments.
3. Design a series of experiments to investigate the effect of different levels of data availability and establish the relationships between data usage and control performance.

In the rest of this paper, section 2 describes the proposed control framework, the testbeds, and the design of virtual and actual experiments. The model and control performance of the basic control framework are presented in section 3, and the results using alternative data points are compared in section 4. Further, section 5 summarizes the takeaways from the experiments and discusses the implications for future research about building energy flexibility and data-centric control.

2. Methodology

2.1. The optimal control framework

Figure 1 displays the implemented control framework that applies model predictive control (MPC) and interacts with the building through a building management system (BMS) interface. The framework consists of three main components: disturbance forecast, control-oriented model, and dynamic optimization. Considering the fast thermal response and small thermal mass of tropical buildings, MPC was configured with 15-minute intervals and 1-hour horizons. The horizon could be prolonged for buildings with larger thermal mass or energy storage systems.

2.1.1. Disturbance forecast

At each time step during operating hours, the control framework started by forecasting the disturbances for the coming control horizon, which was then used as boundary conditions for the control optimization. There were four variables to be forecasted: outdoor temperature, solar irradiance, PV generation, and plug load. Considering that the horizon of one hour is relatively short, the forecasting was purely based on historical data and time. One-step-ahead forecasting was applied recursively (i.e. the forecasted value of the current time step serves as an input for the next time step) four times to form the forecast of one hour.

Long Short-Term Memory (LSTM), a state-of-the-art recurrent neural network for weather forecasting [40], was adopted here for the outdoor temperature and solar irradiance. Historical data and timestamps during the past two hours (eight timesteps) were taken as model inputs. For preprocessing, historical values were standardized, and timestamps were transformed into a cosine signal of a 24-hour period. Two models were trained respectively for temperature and

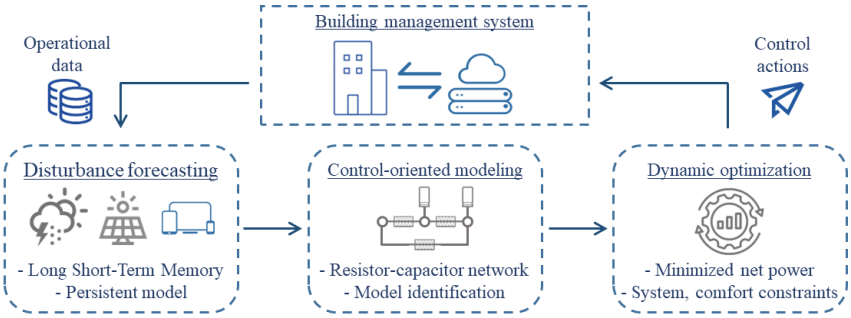

Figure 1: Schematic of the proposed control framework.

irradiance with one year of historical data. Given the high linear correlation between solar irradiance and PV generation, the PV forecast was obtained by multiplying the irradiance forecast by a constant coefficient obtained via regression. Lastly, the persistent model was applied for the plug load forecast since it possessed less complicated temporal patterns.

2.1.2. Control-oriented model

Resistor-capacitor (RC) network is a typical type of control-oriented model that simplifies the building thermal dynamics with a circuit and identifies the RC values through parameter estimation [41]. The complexity of the RC network varies in different cases, and sub-models in figure 2 were aggregated to model the multi zones in this study. Each thermal zone was modeled by the R2C2 room, where R_{ext} stood for the external wall, two capacitors C_{air} and C_{int} respectively represented indoor air and internal mass (floor and ceiling included), and R_{int} was the resistance of convective heat transfer. Model inputs included outdoor temperature T_{out}, internal heat gain Q_{int}, cooling heat flow Q_{clg}, and solar irradiance H_{solar} (heat gain coefficient a to be estimated). Note that Q_{clg} was approximated using supply air temperature T_{SA} and airflow rate $\dot{V}_{SA}$, smaller than the chilled water power P_{clg} measured by BTU meters. This is because the latent cooling load brought by the fresh air was dealt with at the cooling coil and did not affect the heat balance of the rooms. The R2C1 partition modeled the internal walls that connect two neighboring zones with two resistors and one capacitor. Note that the external walls were modeled as one resistor in this study because they are mostly high-performance glasses with negligible thermal capacitance. The R2C1 model should be used if external walls have a larger thermal mass.

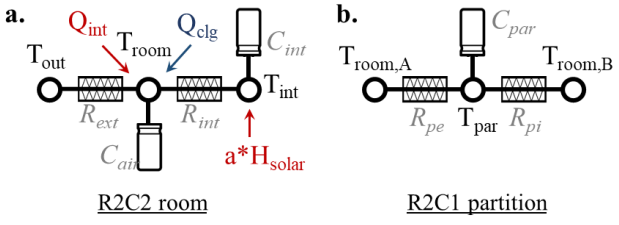

Figure 2: Components used to form the RC network model.

The RC values and solar heat gain coefficients were identified by minimizing the average Root Mean Squared Error (RMSE) of the room temperatures. As shown in equation 1, $T_{RM,i}$ is the measured temperature of the i-th room, $\hat{T}_{RM,i}$ is the room temperature predicted by the RC model (given initial states x, heat flow q, and disturbances d), and the parameters θ are subject to the admissible range $[\theta^{lb}, \theta^{ub}]$. Three days of measured data with a 15-minute interval was used for the identification. The identification was repeated with alternative levels of data availability. Hence, RC models used in the comparative experiments have the same model structure but different parameter values. Given the stable weather conditions in tropical climates, the models were not re-calibrated throughout the experiments.

$$\theta = argmin \int_{t0}^{t1} \sum_{i}^{k} (T_{RM,i} - \hat{T}_{RM,i})^2 dt \tag{1}$$

$$s.t. \quad \widehat{T}_{RM,i} = f(x, q, d, \theta)$$
$$\theta^{lb} \leq \theta \leq \theta^{ub}$$

2.1.3. Dynamic optimization

The goal of MPC was to maximize the local consumption of PV generation and minimize the electricity purchased from the grid. Assuming that the plug load in an office building is not adjustable, the optimization controlled the cooling load according to how much electricity PV generates. Correspondingly, the quadratic objective function 2 minimized the difference between the total building load P_{total} and PV generation P_{PV}. The control variables were the supply airflow rate of each room $\dot{V}_{SA,i}$, which were subject to the physical limitations.

While the room temperatures were constrained to vary between 25 and 28°C, the air movement speed was not included in the optimization considering its minor impact on energy consumption. Although it is theoretically viable to adjust the ceiling fan with respect to the room temperature [42], the actual air movement preference varies across individuals. Considering the high variability of occupants in an open office space, the ceiling fans were left to be adjusted by occupants based on their personal preferences. Meanwhile, as thermal comfort was maintained by different combinations of room temperature and ceiling fan speed, too high air movement speed could increase the discomfort risk of draught (undesirable current of air) [32]. To alleviate this issue, the temperature deviation from $26°C$ (neutral thermal sensation under the default ceiling fan speed) was also penalized with a small weight $q_c = 0.1$. This term enables the optimizer to pursue higher thermal acceptability when there is a spare degree of freedom.

$$J = \int_{t_0}^{t_0+60min} \left((P_{PV} - P_{total})^2 + q_c \sum_{i}^{k} (T_{RM,i} - 26)^2 \right) dt \tag{2}$$
$$s.t. \quad \dot{V}_{SA,min,i} \leq \dot{V}_{SA,i} \leq \dot{V}_{SA,max,i}$$
$$25 \leq T_{RM,i} \leq 28$$

2.1.4. Implementation details

The framework was implemented on a personal desktop that exchanges information with the BMS server through a REpresentational State Transfer (REST) API. The LSTM models were based on TensorFlow[1]. The control-oriented RC models were built using Modelica[2] and compiled into Functional Mock-up Units (FMU)[3] for simulation. Both identification and control optimization were defined in Optimica and solved by the interior-point method (IPOPT) using JModelica[4]. The entire procedure was completed within seconds at each time step.

Although the direct control actions from the optimization were supply airflow rates, it is risky to overwrite the actuators in actual experiments. Therefore, the expected room temperatures at the next timestep were sent to BMS as thermostat setpoints, and the actual airflow rates were still governed by the local Proportional-Integral-Derivative (PID) loop. For consistency, this procedure was also emulated in the virtual experiments.

2.2. Virtual testbed and actual experiments

2.2.1. Building description

The experiments were conducted at 6-zone office spaces located on level 5 of a newly-built net zero energy building in Singapore. The building has a large number of PV panels installed on the rooftop that generates electricity of around the same amount as the building consumes in a year. As displayed in figure 3, the 6-zone spaces consist of four offices and two conference rooms, conditioned by variable air volume (VAV) systems with two dedicated outdoor air fan coil units (FCU). Ceiling fans were installed in each room and controlled by occupants as part of the hybrid cooling system. Table 1 summarizes the information of each room.

During operating hours, the VAV damper positions were modulated by PID loops against the thermostat setpoints. Separate PID loops adjusted the cooling coil valve position and thereby the supply air temperature between 15 and 18°C for each FCU based on the average setpoint of the conditioned zones. Since the optimal control was only applied to part of the building, the total PV generation was allocated to these spaces based on the percentage of energy consumption

[1] https://github.com/tensorflow/tensorflow
[2] https://modelica.org/
[3] https://fmi-standard.org/
[4] https://jmodelica.org/

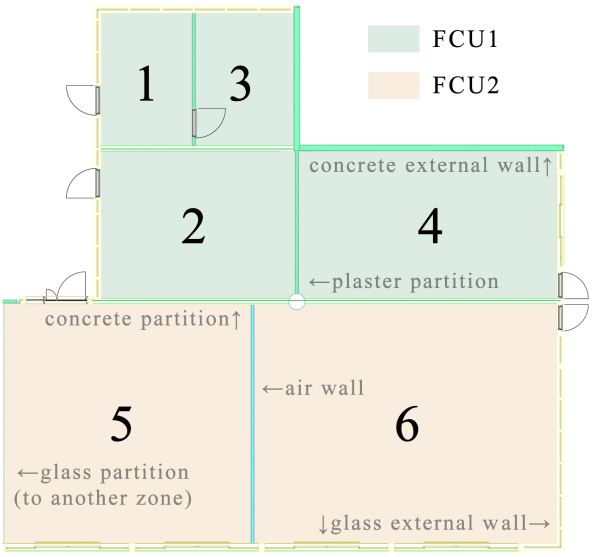

Figure 3: Room layout and constructions of the experiment spaces.

Table 1
Information of the 6 experiment spaces.

No.	*Room function*	*Floor area* $[m^2]$	*Seating capacity*[a]	*FCU*	*Min/max supply airflow rate* $[m^3/h]$[b]
1	Conference	20	4	FCU1	105/210
2	Office	40	4		150/500
3	Office	20	1		150/210
4	Conference	60	10		240/1150
5[c]	Office	81	10	FCU2	175/850
6[c]	Office	99	10		350/1050

[a] The actual number of occupants could temporarily exceed the capacity.
[b] The range of supply airflow rate is based on measured data of each VAV box, different from the specifications.
[c] Room 5 and 6 are in the same big open space but have different thermostats and VAV boxes, and therefore are considered as two thermal zones separated by an air wall.

in the past two years. Figure 4 shows an example of daily consumption and generation profiles of these six zones. It can be seen that PV generation exceeded the total building load around noon and was insufficient in the morning and afternoon. During the experiments, the proposed MPC framework optimized the setpoints to reduce the amount of surplus and purchased energy.

2.2.2. Dataset description

The situation of data availability varies across buildings, and a considerable difference exists in terms of the granularity or resolution of available operational data. Therefore, comparative experiments and scalable applications require a unified method to describe the data usage. The experiment building is very well-metered and has thousands of data points, among which only a small portion is valuable for control. Table 2 summarizes the data points utilized in the MPC framework and investigated in the experiments. The categories were based on a recently proposed extended Level of Detail (LoD) framework [43].

2.2.3. Virtual testbed

A virtual testbed of the experiment spaces was built to lower the experiment cost and enable the comparison of different control strategies under the same boundary conditions. The building thermal dynamics were emulated by an RC model structure similar to the control-oriented model. In addition, PID control loops were replicated and added to the RC model. In the virtual experiments, this emulator takes the optimized setpoints and the boundary conditions as inputs, and reports the resulting power and room temperatures.

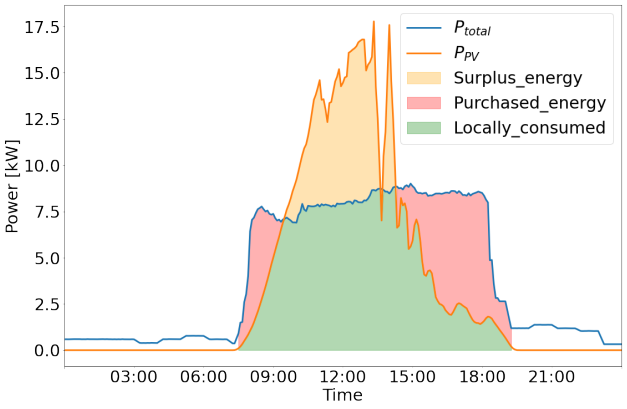

Figure 4: Consumption and generation profiles of the experiment spaces on an example day.

Table 2
Data points involved in the experiments.

Data category[a]	*Point name*	*Symbol*	*Unit*	*Data source*
Energy consumption	chilled water power	P_{clg}	kW	BTU meters of each FCU[b]
	supply air fan power	P_{fan}		power meters of each FCU
	PV power	P_{PV}		smart meter for the entire building[c]
	electric power	P_{elec}		power meters for all zones under each FCU[d]
Indoor condition	room temperature	T_{RM}	°C	thermostats of each room
	CO_2 concentration	C_{CO_2}	ppm	
Internal disturbance	operating schedule	Ope	on/off	building design specifications
	occupant number	Occ		indirect estimation guided by site visit[e]
External disturbance	airport outdoor temperature	$T_{airport}$	°C	airport weather station (~20km away)
	airport solar irradiance	$H_{airport}$	W/m^2	
	local outdoor temperature	T_{local}	°C	rooftop weather station
	local solar irradiance	H_{local}	W/m^2	
System condition	room temperature setpoint	$T_{RM,SP}$	°C	thermostats of each room
	damper position	k_{VAV}	%	VAV boxes of each room
	supply airflow rate	$\dot{V}_{SA}$	m^3/h	airflow meter of each VAV box
	supply air temperature	T_{SA}	°C	off coil temperature sensor of each FCU
	supply air temperature setpoint	$T_{SA,SP}$	°C	PID loop of each cooling coil

[a] The categorization is based on the extended LoD framework proposed in [43]. E.g. internal disturbance includes data points that can be used to estimate occupancy status or internal heat gain.
[b] The BTU meters measured the chiller water heat flow with chiller water temperatures and flow rate, which was converted to chiller plant (chillers and pumps included) electric power with a contract-based COP (Coefficient of Performance) of 5.84.
[c] PV power was allocated to the experiment spaces based on the percentage of historical energy consumption.
[d] Lighting, plug load, and ceiling fan power for zones under the same FCU are measured together.
[e] The real-time occupant number of each zone was approximated based on its P_{elec} and C_{CO_2}. Hereafter, the use of Occ also involves these two variables. Linear relationships were assumed with the peak value corresponding to the maximum occupant number of seating capacity.

To serve as the actual building in the virtual control experiments requires the emulator to accurately predict both the energy and thermal response of the building. Figure 5 compares the emulator outputs and measured data on three consecutive days, where well-matched results can be observed. Testing the model against one month of measured data returned RMSE of 0.65kW for total power (coefficient of variation of 17.60%) and 0.23°C for the room temperatures.

2.3. Design of experiments

2.3.1. Virtual experiments

The control framework was first tested for a month on the virtual testbed. In the simulation, the emulator was initialized at 12am of each day and ran for 24 hours given the actual boundary conditions (T_{local}, H_{local}, P_{PV}, P_{elec}). The control framework was called at each time step during the operating hours, and the control actions ($T_{RM,SP}$, $T_{SA,SP}$)

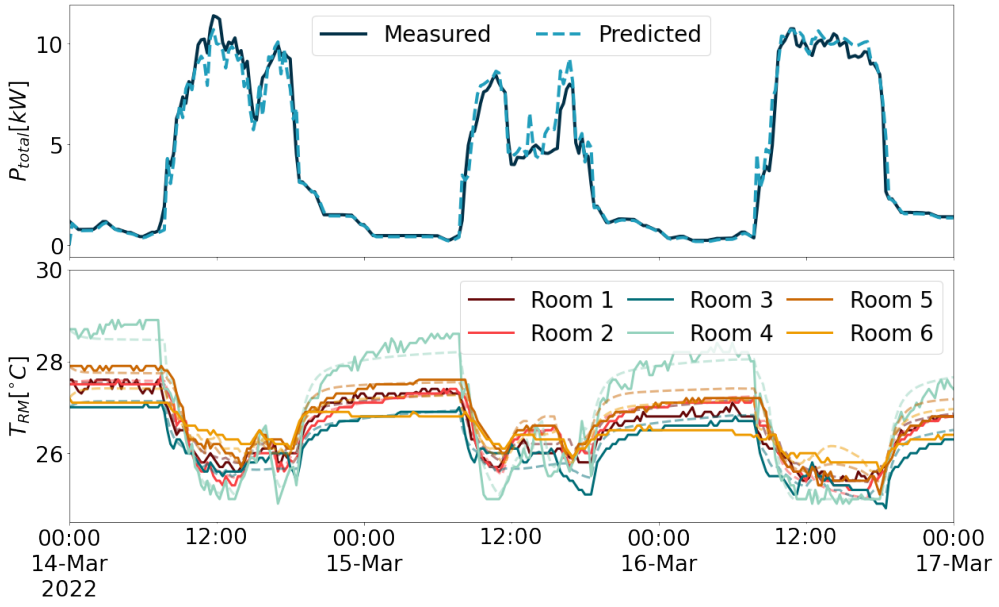

Figure 5: Validation of the predicted total power and room temperatures of the virtual testbed.

Table 3
Control configuration with different levels of data availability.

Case name	*Data points involved in the control framework*		
	Disturbance forecast (input)	*Control-oriented model* (initial state/input)	*Dynamic optimization* (constraint/control action)
`MPC_main`	$T_{local}, H_{local}, P_{PV}, P_{elec}$	$T_{RM}/T_{local}, H_{local}, \dot{V}_{SA}, T_{SA}$	$Ope/T_{RM,SP}$
`MPC_occ`	$T_{local}, H_{local}, P_{PV}, P_{elec}$	$T_{RM}/T_{local}, H_{local}, Occ, \dot{V}_{SA}, T_{SA}$	$Occ/T_{RM,SP}$
`MPC_sat`	$T_{local}, H_{local}, P_{PV}, P_{elec}$	$T_{RM}/T_{local}, H_{local}, \dot{V}_{SA}, T_{SA}$	$Ope/T_{RM,SP}, T_{SA,SP}$
`MPC_airport`	$T_{airport}, H_{airport}, P_{PV}, P_{elec}$	$T_{RM}/T_{airport}, H_{airport}, \dot{V}_{SA}, T_{SA}$	$Ope/T_{RM,SP}$

were applied to advance the simulation. The resulting room temperatures T_{RM} and total power P_{total} were recorded for analysis.

The framework was benchmarked against two baseline control `Base_26` and `Base_27.5` with constant setpoints 26 and 27.5°C. These two setpoints were the previous lower and upper limit of thermostats set during building commissioning. Further, MPC was configured with different levels of data availability as in table 3 for comparison. `MPC_main` is the basic setup. `MPC_occ`, `MPC_airport`, and `MPC_sat` introduce variations in data usage of the category internal disturbance, external disturbance, and system condition.

- `MPC_occ` The occupant numbers of each zone estimated with P_{elec} and C_{CO_2} were used to replace the operating schedule. When identifying the RC model, P_{elec} and C_{CO_2} were used to approximate the internal heat gain with additional coefficients. In the optimization, an extra dynamic constraint of minimum outdoor airflow rate $\dot{V}_{OA,min}$ was applied based on Occ and ASHRAE standard [44]. A safety factor of 1.25 was multiplied to avoid insufficient fresh air.

- `MPC_sat` In the basic setup, $T_{RM,SP}$ was sent to BMS to realize the optimized $\dot{V}_{SA}$, and $T_{SA,SP}$ was governed by the average $T_{RM,SP}$ of zones under each FCU. In this case, T_{SA} was also treated as a control variable in the optimization and $T_{SA,SP}$ was overwritten.

- `MPC_airport` The local ambient conditions measured by the rooftop weather station were assumed to be unavailable. Instead, the airport weather data $T_{airport}$ and $H_{airport}$ were used as a more commonly available data source. Both disturbance forecast and RC modeling were affected.

Another benefit of the virtual testbed is the freedom to alter the building characteristics. Given the dedicated outdoor air systems and the physical restriction of minimum VAV damper positions, the $\dot{V}_{OA,min}$ could make no impact if it is smaller than $\dot{V}_{SA,min}$. Thus, HVAC systems with additional return air ducts and mixing boxes were emulated to investigate the effect of including Occ and $\dot{V}_{OA,min}$, referred to as `MPC_occ_RA`. Similarly, considering that the benefit of having more accurate weather data may be related to how much solar power is generated, the comparison of `MPC_airport` was conducted under various levels of solar power capacity. Under the actual NZEB setting, PV panels were sized to cover 100% of the building's accumulative consumption. In the virtual experiments, solar power abundancy levels of 20, 30, 40, 60, and 80% were also tested.

2.3.2. Actual experiments

Although measured data were used as boundary conditions and the emulator outputs have been validated, the virtual testbed could not fully account for the uncertainties in actual building operation. Besides, the discrepancy between the control-oriented RC model and the emulator was smaller than that in the actual application. Thus, Despite the aforementioned advantages of virtual experiments, the simulation results are to be further validated in reality.

The actual experiments lasted seven weeks since February 2022. Since only one control method can be applied each day, comparing alternative methods under the same boundary conditions is impractical. Although the climate is generally stable in the tropics, it is still possible to have fluctuating ambient conditions and indoor disturbances over the course of two months, making it difficult to properly benchmark the control performance. To robustly test the control methods under various boundary conditions, the six alternatives (`Base_26`, `Base_27.5`, `MPC_main`, `MPC_occ`, `MPC_airport`, and `MPC_sat`) took turns to be applied in a random order.

2.3.3. Performance evaluation

The energy flexibility was reflected in the consumption of PV generation, quantified by two metrics: self-consumption (SC, Equation 3) [45] and self-sufficiency (SS, Equation 4) [10]. In the equations, $E_{locally\_consumed}$ refers to the part of PV generation that is directly consumed on-site (the green area in figure 4), E_{PV} is the daily accumulated PV generation, and E_{total} is daily total energy consumption. Hence, larger SC and SS are both desired.

$$SC = \frac{E_{locally\_consumed}}{E_{PV}} \tag{3}$$

$$SS = \frac{E_{locally\_consumed}}{E_{total}} \tag{4}$$

Apart from energy performance, the accuracy of disturbance forecast and control-oriented models of alternative MPC methods were both evaluated by RMSE. Regarding the indoor environment quality, room temperature constraints could hardly be violated as the PID loops were still taking effect. Thermal comfort was therefore assumed to be guaranteed in the simulation as the ceiling fans could be adjusted instantly.

During actual experiments, comfort surveys were not regularly distributed because 1) most occupants did not regularly stay in the spaces; 2) the experiments were designed to be non-intrusive. Instead, QR codes linked to the survey were provided with a brief notice at the thermostats and entrances of each room. The occupants were informed that they were able to provide feedback within a few clicks. Meanwhile, the CO2 concentration and relative humidity of each room were also monitored.

3. Performance of the control framework

This section demonstrates the effectiveness of the control framework. First, the results of the disturbance forecast and control-oriented model are validated. The control behavior and performance of the basic `MPC_main` are then presented and compared with the baselines. The impact of alternative data availability levels is further investigated in section 4.

3.1. Accuracy of intermediate results

Figure 6 plots the forecasted disturbances of three consecutive days, where the dashed lines are the one-step-ahead forecast, and the solid lines are the measured ground truth. All four variables achieved satisfactory accuracy. The

Table 4
RMSE of the disturbance forecasts during the experiment.

	T_{local} [°C]	H_{local} $[W/m^2]$	$P_{elec,FCU1}$ $[kW]$	$P_{elec,FCU2}$ $[kW]$
1-step-ahead	0.42	108.91	0.07	0.08
2-step-ahead	0.63	123.80	0.13	0.15
3-step-ahead	0.80	131.67	0.18	0.21
4-step-ahead	0.95	137.01	0.21	0.27

two-to-four-step-ahead forecasts were close to the one-step-ahead with slightly larger errors, therefore not included in the figure for better legibility. The RMSE of all variables over the experiment period are summarized in table 4. It is expected to observe the gradually increased RMSE for each variable considering the recursive manner of forecasting, and even the largest four-step-ahead RMSE are competitive compared with the state of the art [46]. All disturbances were measured every minute, and the 15-minute averages were used for analysis. Hence, variations within each minute were not accounted for.

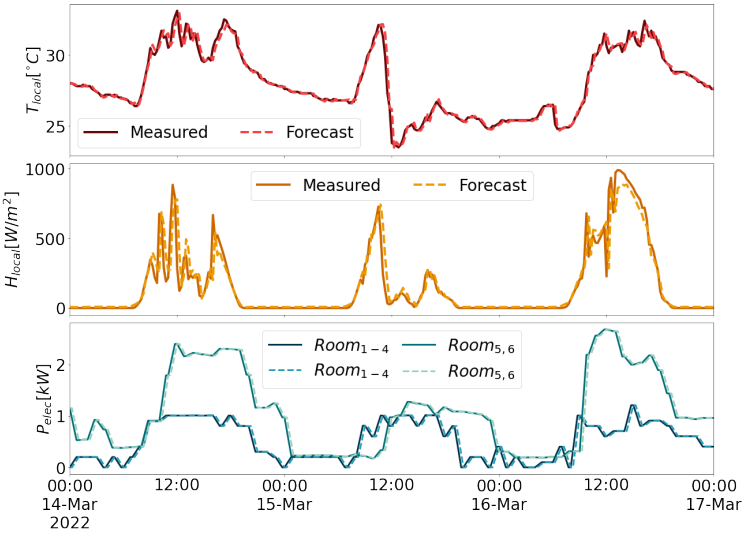

Figure 6: Validation of the disturbance forecast results.

The identified control-oriented models were validated using five days of testing data. The model was initialized with the room temperatures and run for five days given the inputs ($T_{local}, H_{local}, \dot{V}_{SA}, T_{SA}$). This open-loop prediction test was more demanding than the control optimization and guaranteed that the RC models correctly represented the building dynamics. Figure 7 plots the predicted results that matched the measured data. The average RMSE throughout a month was 0.37°C. The error was slightly larger than the virtual testbed as shown in figure 5 due to the absence of PID control loops.

3.2. Typical control behavior

Thirty days of virtual experiments showed that the MPC framework successfully realized the energy flexibility and managed to reduce the discrepancy between P_{PV} and P_{total}. Figure 8 compares the typical control behaviors of `Base_26`, `Base_27.5`, and `MPC_main`. The constant setpoints led to relatively stable P_{total} profiles. Consequently, `Base_26` required electricity purchased from the grid when P_{PV} was insufficient and left a similar amount over when P_{PV} was excessive. `Base_27.5` conservatively reduced the amount of purchased energy by pursuing higher room temperatures, resulting in substantial surplus energy throughout the day. Note that T_{RM} of some zones (especially for `Base_27.5`) often went below the setpoint because of the lower limit of supply airflow rate.

In contrast, both purchased energy (red area) and surplus energy (yellow area) were considerably contracted by `MPC_main`. With the dynamic optimization, the six rooms behaved similarly to match P_{total} with P_{PV}. Instead of abruptly approaching the 26 or 27.5°C setpoints, `MPC_main` started earlier and gradually decreased the room temperatures as P_{PV} increased in the morning. Afterwards, the rooms continued to be cooled down to consume

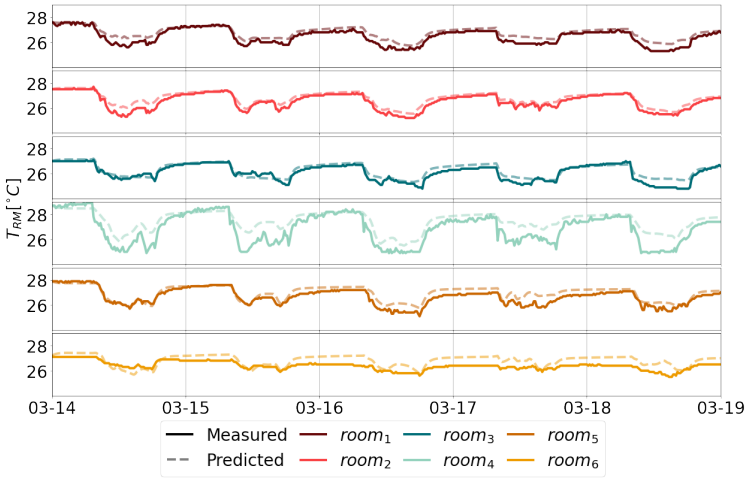

Figure 7: Testing results of the RC model for `MPC_main`.

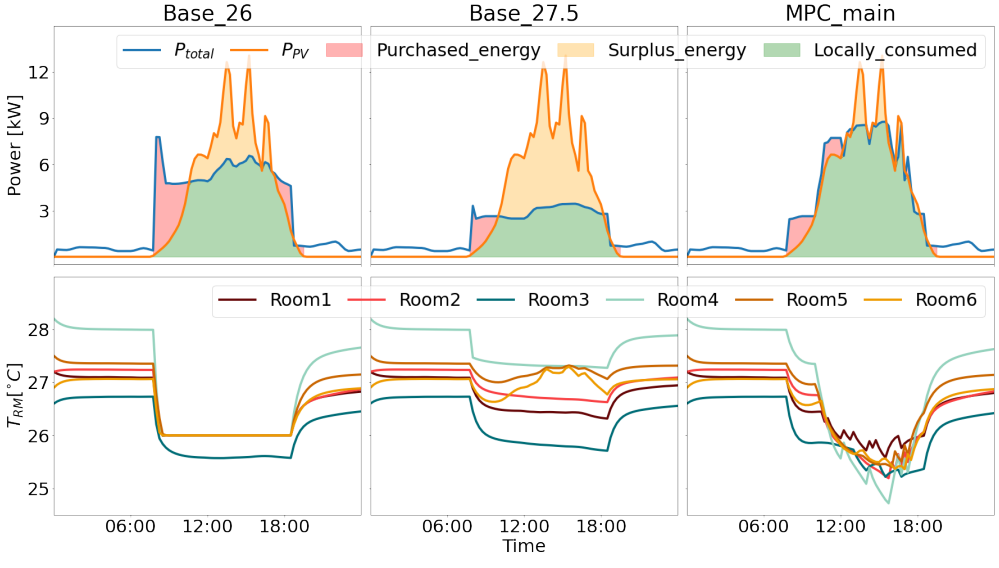

Figure 8: Typical control behaviors of `MPC_main`, compared with `Base_26` and `Base_27.5`.

more PV generation and store some cooling energy in the building's thermal mass. By the end of the daytime, the temperatures slowly bounced back as P_{PV} started to drop. As a result, P_{total} followed P_{PV} most of the time. With the forecasted disturbances, the predictive control precisely increased and decreased the amount of supple air to match the PV generation and maintain the preferable room temperature. These typical behaviors were complied with in the actual experiments. In practice, the remaining mismatch could be caused by 1) the physical limitations, including the minimum supply airflow rate and maximum cooling capacity, 2) the error of disturbance forecast, and 3) the discrepancy between the control-oriented model and the actual building.

Figure 9 illustrates these three causes by comparing the simulation and actual experiment results on a day when P_{PV} fluctuated. The highlighted surplus and purchased energy in the first subplot were respectively caused by the maximum cooling capacity and minimum supply airflow rate. In figure 9.b, it is clear that the forecast of H_{local} was lagged by one time step when the actual measurement suddenly changed. This further led to the error in the PV power forecast and affected the optimization. It is also worth noting a rare situation where H_{local} once suddenly decreased around noon while P_{PV} was stable. These two factors applied to both the virtual and actual experiments.

Figure 9.c shows the mostly consistent simulated and actual control results on this day and highlights the unmatched part, which was caused by the model-reality discrepancy. The last plot compares the actual and expected supply airflow rate of room 5. For example, the control-oriented model underestimated the room temperature and sent a too low

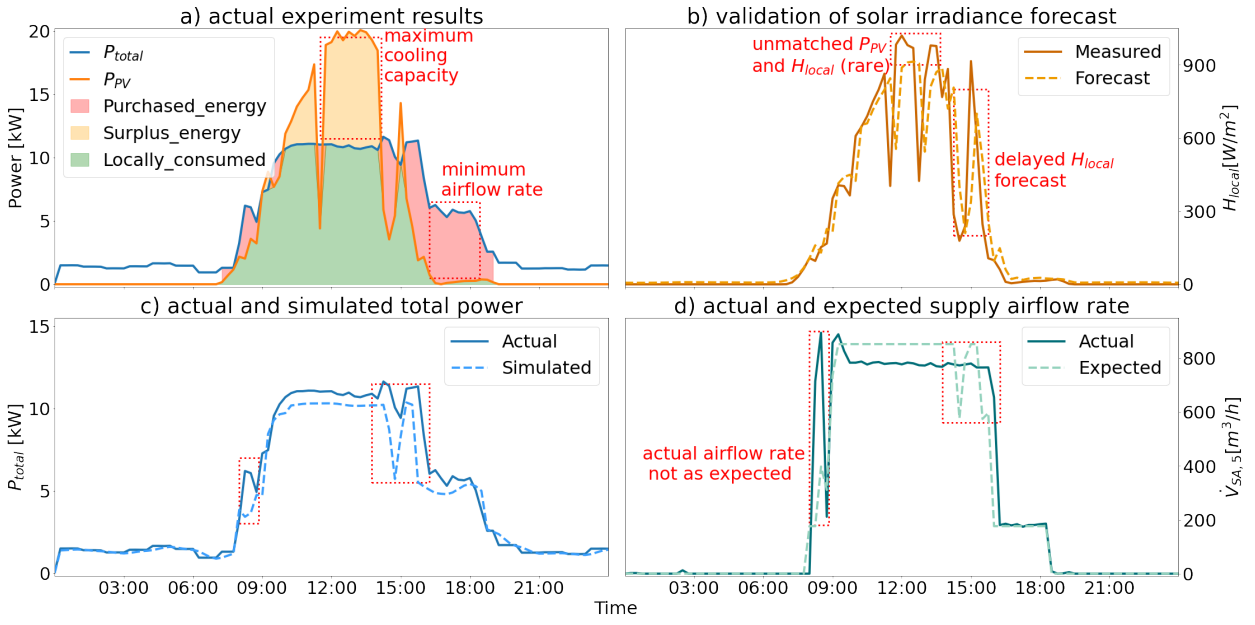

Figure 9: One day of actual experiment results and the causes of undesirable control behaviors.

setpoint in the early morning, causing the leap in supply airflow rate. In the afternoon, the model underestimated the temperature again, raised the setpoint too slowly, and decreased $\dot{V}_{SA,5}$ with a delay.

3.3. Control performance evaluation

The control performance of each day was evaluated by self-consumption (SC) and self-sufficiency (SS). The daily total energy consumption was also calculated for reference. The boxplots in figure 10 visualizes the distributions of the daily evaluation results of `Base_26`, `Base_27.5`, and `MPC_main` in the virtual experiments. The actual experiments ended up with six days for each control method. The evaluation results of each day were marked by dots in figure 10, which had no significant difference from the corresponding simulation results (p-values all greater than 0.05).

The control performance on a specific day is highly dependent on the intensity and pattern of solar irradiance. For example, a larger amount of PV generation usually yields higher SS and lower SC, and fluctuating patterns tend to deteriorate the optimal control performance. Without a proper normalization method, it is not straightforward to directly compare the control performance on different days. Therefore, the simulation and experiment results were combined to form a larger sample size for benchmarking.

Among the two baselines, `Base_26` had obviously higher energy consumption and SC percentage than `Base_27.5`. Meanwhile, their SS showed no significant difference with a p-value of 0.87 in paired t-test. `MPC_main` performed significantly better in both SC and SS (p-values close to zero). Compared with `Base_26`, SC and SS were respectively improved by 19.5% and 10.6%. Although the total energy consumption was also higher, a high percentage of energy was consumed when there was surplus energy, reflected in the higher SS.

The indoor environment was assumed satisfactory in the simulation but closely monitored during the actual experiments. CO_2 concentration below 800ppm was recommended as the ventilation requirement under the covid situation [47]. Over the course of two months, C_{CO_2} of these six rooms never exceeded this threshold, indicating sufficient ventilation and good indoor air quality. The relative humidity measured for each room was stable and around 60% during operating hours. The air movement speed was inferred from the daily energy consumption of ceiling fans. It shows that the ceiling fan speed of `MPC_main` was comparable to `Base_26`, slightly (around 5%) lower than `Base_27.5`.

As for thermal comfort, T_{RM} was normally between 25 and 27.5°C, within the thermal comfort range given the elevated air movement speed. However, two complaints were filed in room 5 around noon on days with baseline control (once with `Base_26`, another with `Base_27.5`). This implies the potential discomfort risk around noon. In this case, the control behavior of lowering the room temperature towards the lower bound (25°C) when solar irradiance was intense also had the benefit of guaranteeing thermal comfort.

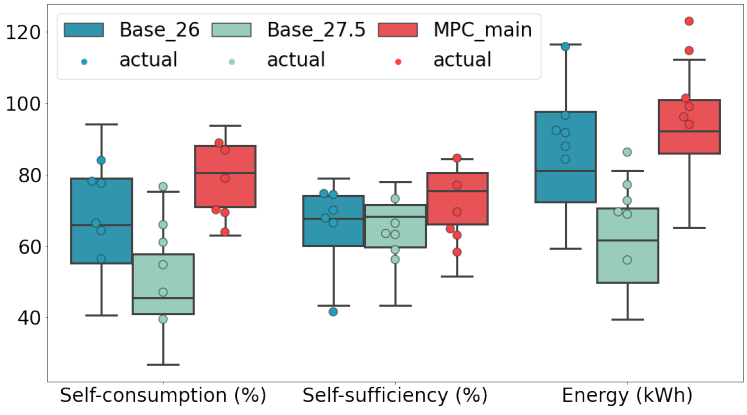

Figure 10: Control performance comparison of `Base_26`, `Base_27.5`, and `MPC_main`.

4. Impact of data availability

Figure 11 summarizes the control performance of alternative MPC configurations in virtual and actual experiments. While `MPC_occ` and `MPC_sat` performed almost the same as `MPC_main`, the two metrics of `MPC_airport` were both worsened. In this section, the impact and underlying mechanisms of each data category are investigated.

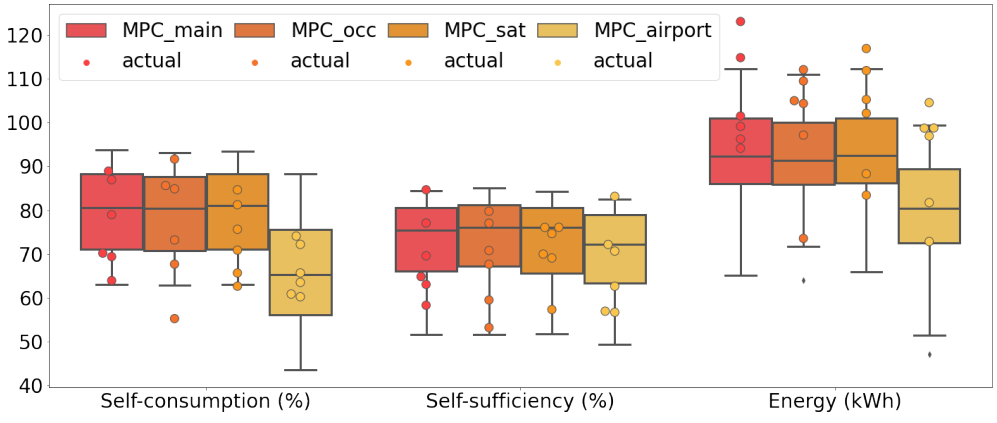

Figure 11: Control performance comparison of `Base_26`, `Base_27.5`, and `MPC_main`.

4.1. Internal disturbance

The first change under this category was to include the two related data sources P_{elec} and C_{CO_2} as RC model inputs. The resulting model performance was not significantly different from figure 7, yielding an average RMSE of 0.39°C. This marginal difference was negligible in the control horizon of one hour. The RC model did not benefit from this addition because 1) the experiment site is part of an NZEB with relatively low internal load density (occupant, plug, and lighting), and the model discrepancy mainly lay in the building thermal dynamics; 2) the exact internal heat gain was unmeasured and highly uncertain, and the data sources could only provide a rough estimation.

The estimated occupant numbers Occ were also used to update the outdoor air constraint $\dot{V}_{OA,min}$ in dynamic optimization, which turned out to be indistinguishable from `MPC_main` under the dedicated outdoor air setting. Figure 12 manifests this influence with the control behaviors of room 5 on a typical day. As $\dot{V}_{OA,min}$ was constantly lower than $\dot{V}_{SA,min}$ and did not affect the control decisions, `MPC_occ` yielded almost identical results as `MPC_main`. A traditional HVAC system with return air `MPC_occ_RA` was emulated to decouple these two constraints, where $\dot{V}_{OA}$ could be further lowered by the mixing box damper position when $\dot{V}_{SA}$ was restricted. As shown in the middle plot of figure 12, the $\dot{V}_{OA}$ of `MPC_occ_RA` was slightly lower than the other two methods when P_{PV} was low. This reduced the chilled water consumption, as highlighted by the yellow area in the top plot. Intuitively, less purchased energy improved self-sufficiency. Meanwhile, the flexibility also brought a greater risk of falsely lowering the self-consumption due to forecast error. Throughout the virtual experiment, `MPC_occ_RA` improved SS by 2.8% and decreased SC by 1.2%.

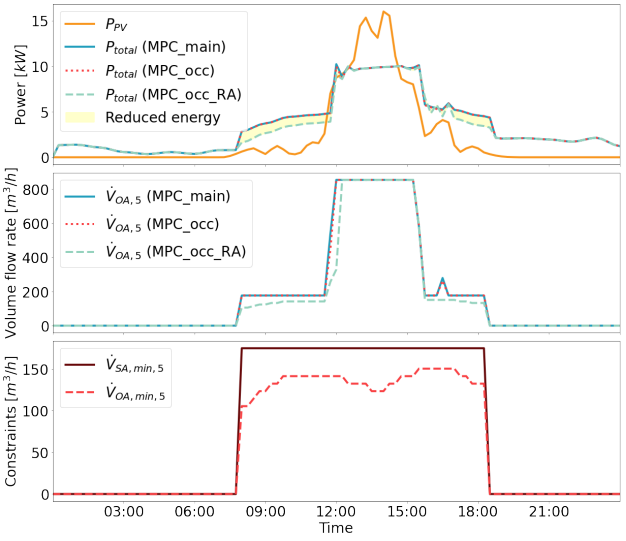

Figure 12: Typical control behaviors of `MPC_main`, `MPC_occ`, and `MPC_occ_RA`.

4.2. System condition

The control-oriented model of `MPC_sat` was the same as `MPC_main` because $\dot{V}_{SA}$, and T_{SA} were found indispensable. For air-based systems, the latent heat removed at the cooling coil does not contribute to the Q_{clg} delivered to the rooms. Thus, the chilled water power P_{clg} was not suitable as RC model inputs, and $\dot{V}_{SA}$ was used to estimate Q_{clg}. Theoretically, $\dot{V}_{SA}$ can be estimated by the damper position feedback k_{VAV} in the common absence of airflow meters. However, the actual nominal airflow rate often deviates from the design documentation, and attention should be paid in practice to acquire the as-built information.

As the primary control objective was to match P_{total} with P_{PV}, the resulting energy behavior was driven by the abundancy of PV generation. Consequently, `MPC_main` and `MPC_sat` made no significant difference in the energy performance. As shown in figure 13, the two P_{total} profiles were very similar. Meanwhile, distinct control actions of T_{SA} were taken, and the room temperature of `MPC_sat` was closer to $26°C$. With `MPC_sat`, T_{SA} was pushed to the lower bound $15°C$ to accelerate the cooling and raised to $18°C$ when T_{RM} was around or lower than $26°C$. In contrast, the T_{SA} of `MPC_main` generally followed the trend of T_{RM} to be decreased till late afternoon and then increased. Thus, while $T_{RM,SP}$ was set to adjust $\dot{V}_{SA}$ and fulfill the energy flexibility requests, controlling T_{SA} separately allows the optimizer to compensate for the change of $\dot{V}_{SA}$ and to pursue independent room temperature setpoints.

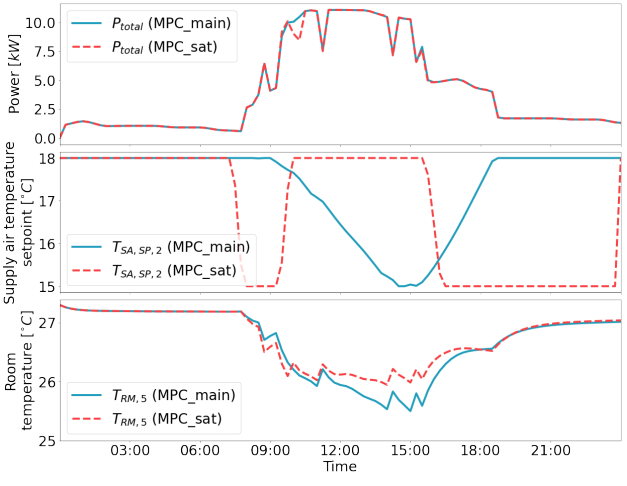

Figure 13: Typical control behaviors of `MPC_main` and `MPC_sat`.

4.3. External disturbance

Surprisingly, using $T_{airport}$ and $H_{airport}$ instead of T_{local} and H_{local} as RC model inputs did not deteriorate the model accuracy. The parameter values estimated by Equation 1 and the predicted temperature response during the same period as figure 7 were close to `MPC_main`, achieving an average RMSE of 0.36°C. There are two possible reasons. First, Figure 14 compares the airport and local weather data in a week. Despite the noticeable error (RMSE of 1.33°C and 203.5W/m^2), the airport data usually followed the trend of local weather, especially for T_{out}. Besides, the building envelope, well-shaded high-performance glasses, had low thermal conductivity and solar heat gain coefficients, which effectively diminished the impact of outdoor conditions.

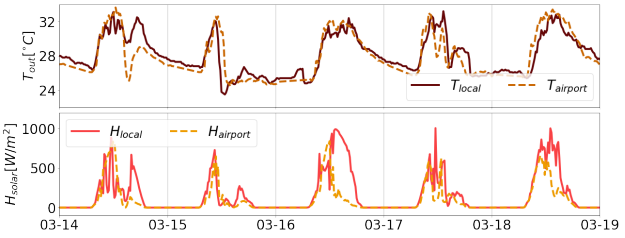

Figure 14: One week of airport and local weather data.

Although $T_{airport}$ and $H_{airport}$ caused no problem to the control-oriented model, it is straightforward that the weather forecast error was significantly enlarged. The RMSE of one-step-ahead forecasts were 1.58° for T_{out} and 201.9W/m^2 for H_{solar}. Unlike the RC model, the dynamic optimization was very sensitive to the forecast of H_{solar} and P_{PV}. When P_{PV} was underestimated, P_{total} would be falsely lowered, which harms self-consumption. Similarly, self-sufficiency would be interfered with by overestimated P_{PV}. As P_{total} was capped by the cooling capacity, the self-sufficiency was only mildly degraded. Interestingly, $H_{airport}$ was at an overall lower level than H_{local}, resulting in lower total energy consumption.

Considering that an on-site weather station is expensive and rare, parametric simulation studies were conducted to evaluate the benefit under various levels of PV capacity. The average SS and SC under different situations are plotted in figure 15. It is expected that SC increased and SS decreased as the PV capacity was lower, and the gaps between `MPC_main` and `MPC_airport` were also contracted. The mild advantage of `MPC_main` in SS vanished when the abundancy level was lower than 50%. As for self-consumption, the need for precise control to improve local consumption was weakened by low PV generation. The benefit of having on-site weather data disappeared when the abundancy went below 20%.

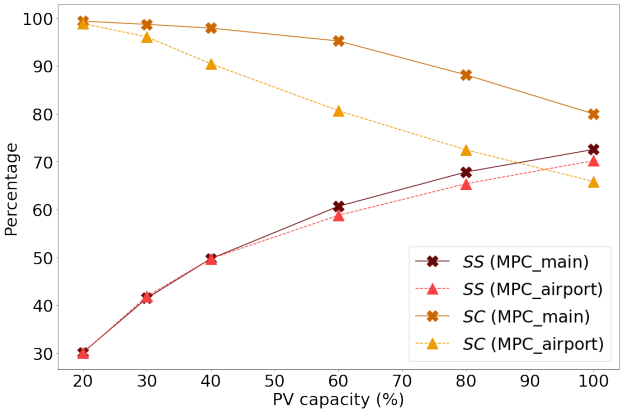

Figure 15: Self-consumption and self-sufficiency of `MPC_main` and `MPC_airport` under different PV capacity levels.

5. Discussion

5.1. Energy flexibility of tropical office buildings

The experiment results demonstrate the energy flexibility enabled by the hybrid cooling systems and the MPC framework. The improvement in self-consumption and self-sufficiency indicates that the building successfully regulated its electricity load to align with the profile of PV generation. The flexibility was realized by continuously adjusting the cooling setpoints within the thermal comfort range. The occupants found such dynamic indoor environments satisfactory during the actual experiments, which agreed with the observations made by Liu and Heiselberg [48]. Moreover, many studies have shown that a stable thermal environment with tight temperature control is not preferable in practice [49].

Although the case study was conducted in a net zero energy building, the benefit was shown to remain at lower PV abundancy levels. Fundamentally, the MPC framework enables the energy flexibility to adjust building electricity loads based on predictive boundary conditions. This capability can be utilized in many control scenarios other than improving PV self-consumption. For example, the objective function of MPC can be defined as the energy cost to incorporate time-varying energy prices and satisfy demand response requests from the grid. In these scenarios, the electricity loads are sometimes deliberately increased, which causes higher energy use but reliefs the pressure on grid operations. On the other hand, self-consumption was improved in this study by simply lowering the temperature setpoint, leading to unnecessary energy use. To further improve energy performance, it is possible to charge energy storage systems (ESS) with surplus PV generation for later use.

Another limitation of not involving batteries in the energy systems is that neither SS nor SC could achieve 100%. It was inevitable to sell or purchase electricity, and the building could not be operated completely off-grid. Further improvements could be driven by integrating different physical systems. For example, ESS could be involved to shift the PV generation over a couple of hours or even days with a longer control horizon. It is worth noting the necessity of an integrative framework to optimize the energy systems from design to operation [50]. Also, day-ahead power forecast and planning would be desired to fully realize the benefit [51]. Besides, it is possible to get higher SS by switching buildings to natural ventilation under appropriate conditions [52].

5.2. Towards data-centric optimal control

While the energy flexibility was provided by the building systems and the control framework, the experiments showed the importance of data in realizing the potential. In other words, the physical systems set the upper limit of the control performance, and the data availability decides the actual performance in practice. It was also recognized that additional data points did not always bring better performance. Considering that data could be very expensive, wisely choosing the data points to collect is crucial for the success of control. Hence, we propose a "data-centric" framework for real-world MPC projects.

The blue part in figure 16 illustrates the traditional paradigm of "model-centric" MPC. The acquisition of operational data is usually performed once when commissioning the building, either arbitrarily or just for monitoring. The data is used for MPC configuration after processing, where most of the development effort is devoted to constructing a fit model [34]. Many model-centric studies have achieved desirable control performance, which, however, is subject to the specific building characteristics and data availability of each study. Consequently, these results can hardly be reproduced, and a high level of customization is required for every new building [33].

In contrast, the data-centric MPC workflow starts with control-oriented data curation that selects which data points to collect through cost-effectiveness analysis. This procedure is different from feature selection, as one common step of data processing, that only considers the predictive model accuracy and is usually based on statistical measures. By control-oriented, the analysis accounts for the integrative impact of data points on the downstream model and control performance, which are affected by many factors such as the building characteristic and the data usage. For example, occupant number estimation showed no superiority under dedicated outdoor air systems, and the local weather data improved PV generation forecast but not RC model accuracy. Hence, making such informed decisions is not straightforward, calling for a comprehensive understanding of the relationship between data usage and control performance. Data-centric evaluation is essential to establish such quantitative relationships. Denoted as dashed lines in figure 16, the evaluation experiments are not part of the workflow in actual applications but experiments to be carried on beforehand in proof-of-concept studies.

MPC was adopted in this study, but the data-centric framework could incorporate other optimal control methods such as reinforcement learning. Although the data curation is an additional step upon the original workflow, it has

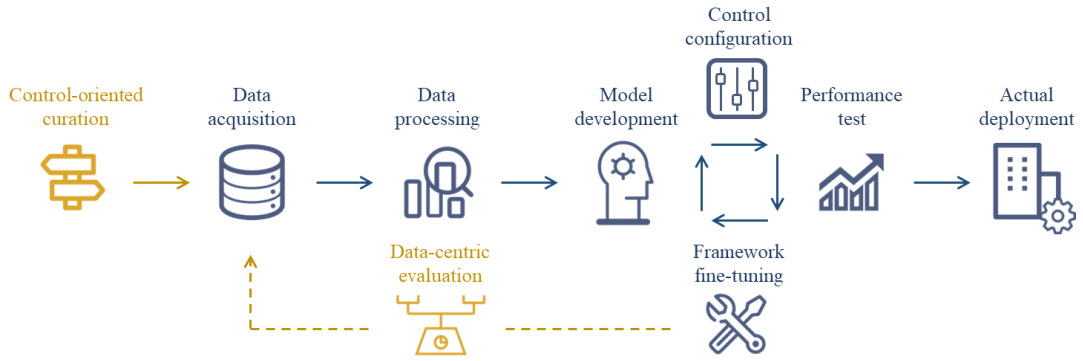

Figure 16: Schematic of a data-centric control framework.

manifold benefits for the downstream configurations. An established end-to-end workflow can be reproduced with less effort devoted to model development and control configuration [39]. The acquisition cost of unnecessary data points can also be avoided. Thereby, the investment and expected outcome of a control project can be better evaluated, which is critical for real-world implementations. This study serves as an example of data-centric evaluation, the conclusions of which are generalizable for tropical office buildings. Future research is required to conduct the data-centric evaluation for other control scenarios and consolidate the corresponding data-centric workflow.

6. Conclusion

This paper proposed a practical optimal control framework that realizes the energy flexibility of tropical office buildings and improves the local consumption of PV generation. The proposed framework was implemented and benchmarked against two baseline controls with constant setpoints in both virtual and actual experiments. Based on the experiment results, the framework successfully regulated the electricity load to align with the PV generation. The PV self-consumption and building self-sufficiency were respectively 19.5% and 10.6% higher than the baseline control of 26°C setpoint.

Additionally, MPC configured with alternative levels of data availability was compared. The mechanisms of different data points taking effect were investigated by examining the intermediate and final results of the control framework. Three categories of data were tested, including internal disturbance, external disturbance, and system condition. It turned out that weather data had the most significant impact as disturbance forecasting was the most sensitive to data sources. Furthermore, the impact of data was inspected under varied building characteristics in simulation to better understand when and why higher granularity or accuracy could be beneficial. For example, the benefit of a local weather station became marginal as the PV capacity decreased.

According to the experiment results, we proposed shifting the MPC workflow from the traditional model-centric to data-centric. The new workflow starts with control-oriented data curation, where the desired data points are determined based on the control purpose and building characteristics. This additional step promotes the scalability of MPC by acquiring data cost-effectively and saving downstream configuration efforts. Making informed decisions requires the end-to-end relationships between data availability and control performance, which is established by systematic experiments as shown in this paper. Therefore, further research is needed to obtain the understanding of other building types and control scenarios.

CRediT authorship contribution statement

Sicheng Zhan: Conceptualization,Methodology,Data Curation,Formal analysis,Investigation,Visualization,Writing - Original Draft, Writing - Review & Editing. **Bing Dong:** Conceptualization, Writing - Review & Editing. **Adrian Chong:** Conceptualization, Supervision, Writing - Review & Editing.

Acknowledgement

We thank Johnson Controls OpenBlue Innovation Center and the Division of Industrial Design (National University of Singapore) for participating and allowing us to conduct our study in their offices.

References

[1] F. Gökgöz, M. T. Güvercin, Energy security and renewable energy efficiency in eu, Renewable and Sustainable Energy Reviews 96 (2018) 226–239. doi:10.1016/j.rser.2018.07.046.

[2] IEA, Global Energy Review 2021, Technical Report, International Energy Agency, 2021.

[3] O. Gandhi, D. S. Kumar, C. D. Rodríguez-Gallegos, D. Srinivasan, Review of power system impacts at high pv penetration part i: Factors limiting pv penetration, Solar Energy 210 (2020) 181–201. doi:10.1016/j.solener.2020.06.097.

[4] Q. Cui, L. He, G. Han, H. Chen, J. Cao, Review on climate and water resource implications of reducing renewable power curtailment in china: A nexus perspective, Applied Energy 267 (2020) 115114. doi:10.1016/j.apenergy.2020.115114.

[5] I. Hamilton, H. Kennard, O. Rapf, J. Kockat, D. S. Zuhaib, 2020 Global Status Report for Buildings and Construction, Technical Report, United Nations Environment Programme, 2020.

[6] I. PVPS, Snapshot of Global PV Markets 2021, Technical Report, International Energy Agency Photovoltaic Power Systems Programme (PVPS), 2021.

[7] Q. Hou, N. Zhang, E. Du, M. Miao, F. Peng, C. Kang, Probabilistic duck curve in high pv penetration power system: Concept, modeling, and empirical analysis in china, Applied Energy 242 (2019) 205–215. doi:10.1016/j.apenergy.2019.03.067.

[8] H. Fontenot, B. Dong, Modeling and control of building-integrated microgrids for optimal energy management–a review, Applied Energy 254 (2019) 113689. doi:10.1016/j.apenergy.2019.113689.

[9] R. Luthander, J. Widén, D. Nilsson, J. Palm, Photovoltaic self-consumption in buildings: A review, Applied energy 142 (2015) 80–94. doi:10.1016/j.apenergy.2014.12.028.

[10] R. Luthander, A. M. Nilsson, J. Widén, M. Åberg, Graphical analysis of photovoltaic generation and load matching in buildings: A novel way of studying self-consumption and self-sufficiency, Applied Energy 250 (2019) 748–759. doi:10.1016/j.apenergy.2019.05.058.

[11] G. Reynders, R. A. Lopes, A. Marszal-Pomianowska, D. Aelenei, J. Martins, D. Saelens, Energy flexible buildings: An evaluation of definitions and quantification methodologies applied to thermal storage, Energy and Buildings 166 (2018) 372–390. doi:10.1016/j.enbuild.2018.02.040.

[12] C. Yan, W. Shi, X. Li, Y. Zhao, Optimal design and application of a compound cold storage system combining seasonal ice storage and chilled water storage, Applied Energy 171 (2016) 1–11. doi:10.1016/j.apenergy.2016.03.005.

[13] S. K. Shah, L. Aye, B. Rismanchi, Seasonal thermal energy storage system for cold climate zones: A review of recent developments, Renewable and Sustainable Energy Reviews 97 (2018) 38–49. doi:10.1016/j.rser.2018.08.025.

[14] G. Bruni, S. Cordiner, V. Mulone, V. Sinisi, F. Spagnolo, Energy management in a domestic microgrid by means of model predictive controllers, Energy 108 (2016) 119–131. doi:10.1016/j.energy.2015.08.004.

[15] L. Bartolucci, S. Cordiner, V. Mulone, M. Santarelli, Hybrid renewable energy systems: Influence of short term forecasting on model predictive control performance, Energy 172 (2019) 997–1004. doi:10.1016/j.energy.2019.01.104.

[16] Y. Chen, P. Xu, J. Gu, F. Schmidt, W. Li, Measures to improve energy demand flexibility in buildings for demand response (dr): A review, Energy and Buildings 177 (2018) 125–139. doi:10.1016/j.enbuild.2018.08.003.

[17] IEA, Energy storage, Technical Report, International Energy Agency, 2021.

[18] J. M. Raya-Armenta, N. Bazmohammadi, J. G. Avina-Cervantes, D. Saez, J. C. Vasquez, J. M. Guerrero, Energy management system optimization in islanded microgrids: An overview and future trends, Renewable and Sustainable Energy Reviews 149 (2021) 111327. doi:10.1016/j.rser.2021.111327.

[19] G. Aghajani, H. Shayanfar, H. Shayeghi, Presenting a multi-objective generation scheduling model for pricing demand response rate in micro-grid energy management, Energy Conversion and Management 106 (2015) 308–321. doi:10.1016/j.enconman.2015.08.059.

[20] J. Lizana, D. Friedrich, R. Renaldi, R. Chacartegui, Energy flexible building through smart demand-side management and latent heat storage, Applied energy 230 (2018) 471–485. doi:10.1016/j.apenergy.2018.08.065.

[21] K. Zhang, M. Kummert, Evaluating the impact of thermostat control strategies on the energy flexibility of residential buildings for space heating, Building Simulation 14 (2021) 1439–1452. doi:10.1007/s12273-020-0751-x.

[22] S. Ø. Jensen, A. Marszal-Pomianowska, R. Lollini, W. Pasut, A. Knotzer, P. Engelmann, A. Stafford, G. Reynders, Iea ebc annex 67 energy flexible buildings, Energy and Buildings 155 (2017) 25–34. doi:10.1016/j.enbuild.2017.08.044.

[23] H. Tang, S. Wang, H. Li, Flexibility categorization, sources, capabilities and technologies for energy-flexible and grid-responsive buildings: State-of-the-art and future perspective, Energy 219 (2021) 119598. doi:10.1016/j.energy.2020.119598.

[24] M. Shafie-Khah, M. Kheradmand, S. Javadi, M. Azenha, J. de Aguiar, J. Castro-Gomes, P. Siano, J. Catalão, Optimal behavior of responsive residential demand considering hybrid phase change materials, Applied Energy 163 (2016) 81–92. doi:10.1016/j.apenergy.2015.11.013.

[25] K. Foteinaki, R. Li, T. Péan, C. Rode, J. Salom, Evaluation of energy flexibility of low-energy residential buildings connected to district heating, Energy and Buildings 213 (2020) 109804. doi:10.1016/j.enbuild.2020.109804.

[26] S. Aghniaey, T. M. Lawrence, The impact of increased cooling setpoint temperature during demand response events on occupant thermal comfort in commercial buildings: A review, Energy and Buildings 173 (2018) 19–27. doi:10.1016/j.enbuild.2018.04.068.

[27] M. Pothitou, R. F. Hanna, K. J. Chalvatzis, Ict entertainment appliances' impact on domestic electricity consumption, Renewable and Sustainable Energy Reviews 69 (2017) 843–853. doi:10.1016/j.rser.2016.11.100.

[28] R. D'hulst, W. Labeeuw, B. Beusen, S. Claessens, G. Deconinck, K. Vanthournout, Demand response flexibility and flexibility potential of residential smart appliances: Experiences from large pilot test in belgium, Applied Energy 155 (2015) 79–90. doi:10.1016/j.apenergy.2015.05.101.

[29] W. Feng, Q. Zhang, H. Ji, R. Wang, N. Zhou, Q. Ye, B. Hao, Y. Li, D. Luo, S. S. Y. Lau, A review of net zero energy buildings in hot and humid climates: Experience learned from 34 case study buildings, Renewable and Sustainable Energy Reviews 114 (2019) 109303. doi:10.1016/j.rser.2019.109303.

[30] H. Li, Z. Wang, T. Hong, M. A. Piette, Energy flexibility of residential buildings: A systematic review of characterization and quantification methods and applications, Advances in Applied Energy 3 (2021) 100054. doi:10.1016/j.adapen.2021.100054.

[31] K. Sudhakar, M. Winderl, S. S. Priya, Net-zero building designs in hot and humid climates: A state-of-art, Case Studies in Thermal Engineering 13 (2019) 100400. doi:10.1016/j.csite.2019.100400.

[32] K. Mihara, C. Sekhar, Y. Takemasa, B. Lasternas, K. W. Tham, Thermal comfort and energy performance of a dedicated outdoor air system with ceiling fans in hot and humid climate, Energy and Buildings 203 (2019) 109448. doi:10.1016/j.enbuild.2019.109448.

[33] J. Drgoňa, J. Arroyo, I. C. Figueroa, D. Blum, K. Arendt, D. Kim, E. P. Ollé, J. Oravec, M. Wetter, D. L. Vrabie, et al., All you need to know about model predictive control for buildings, Annual Reviews in Control 50 (2020) 190 – 232. doi:10.1016/j.arcontrol.2020.09.001.

[34] G. A. Benndorf, D. Wystrcil, N. Réhault, Energy performance optimization in buildings: A review on semantic interoperability, fault detection, and predictive control, Applied Physics Reviews 5 (2018) 041501. doi:10.1063/1.5053110.

[35] A. Chong, K. Menberg, Guidelines for the bayesian calibration of building energy models, Energy and Buildings 174 (2018) 527 – 547. URL: publication/pdf/chong-2018527.pdf. doi:10.1016/j.enbuild.2018.06.028.

[36] K. Amasyali, N. M. El-Gohary, A review of data-driven building energy consumption prediction studies, Renewable and Sustainable Energy Reviews 81 (2018) 1192–1205. doi:10.1016/j.rser.2017.04.095.

[37] Y. Bae, S. Bhattacharya, B. Cui, S. Lee, Y. Li, L. Zhang, P. Im, V. Adetola, D. Vrabie, M. Leach, et al., Sensor impacts on building and hvac controls: A critical review for building energy performance, Advances in Applied Energy (2021) 100068. doi:10.1016/j.adapen.2021.100068.

[38] S. Zhan, Y. Lei, Y. Jin, D. Yan, A. Chong, Impact of occupant related data on identification and model predictive control for buildings, Applied Energy 323 (2022) 119580. doi:10.1016/j.apenergy.2022.119580.

[39] D. Blum, Z. Wang, C. Weyandt, D. Kim, M. Wetter, T. Hong, M. A. Piette, Field demonstration and implementation analysis of model predictive control in an office hvac system, Applied Energy 318 (2022) 119104. doi:10.1016/j.apenergy.2022.119104.

[40] C. Voyant, G. Notton, S. Kalogirou, M.-L. Nivet, C. Paoli, F. Motte, A. Fouilloy, Machine learning methods for solar radiation forecasting: A review, Renewable Energy 105 (2017) 569–582. doi:10.1016/j.renene.2016.12.095.

[41] E. Atam, L. Helsen, Control-oriented thermal modeling of multizone buildings: methods and issues: intelligent control of a building system, IEEE Control Systems Magazine 36 (2016) 86–111. doi:10.1109/MCS.2016.2535913.

[42] Y. Lei, S. Zhan, E. Ono, Y. Peng, Z. Zhang, T. Hasama, A. Chong, A practical deep reinforcement learning framework for multivariate occupant-centric control in buildings, Applied Energy 324 (2022) 119742. doi:10.1016/j.apenergy.2022.119742.

[43] S. Zhan, A. Chong, Data requirements and performance evaluation of model predictive control in buildings: A modeling perspective, Renewable and Sustainable Energy Reviews (2021) 110835. doi:10.1016/j.rser.2021.110835.

[44] ANSI/ASHRAE, ANSI/ASHRAE Standard 62.1-2019: Ventilation for acceptable indoor air quality, 2019.

[45] M. Jaszczur, Q. Hassan, A. M. Abdulateef, J. Abdulateef, Assessing the temporal load resolution effect on the photovoltaic energy flows and self-consumption, Renewable Energy 169 (2021) 1077–1090. doi:10.1016/j.renene.2021.01.076.

[46] B. Dong, R. Widjaja, W. Wu, Z. Zhou, Review of onsite temperature and solar forecasting models to enable better building design and operations, Building Simulation 14 (2021) 885–907. doi:10.1007/s12273-020-0759-2.

[47] C. for Disease Control, Prevention, Ventilation in buildings, 2022. URL: https://www.cdc.gov/coronavirus/2019-ncov/community/ventilation.html.

[48] M. Liu, P. Heiselberg, Energy flexibility of a nearly zero-energy building with weather predictive control on a convective building energy system and evaluated with different metrics, Applied Energy 233 (2019) 764–775. doi:10.1016/j.apenergy.2018.10.070.

[49] Y. Zhu, Q. Ouyang, B. Cao, X. Zhou, J. Yu, Dynamic thermal environment and thermal comfort, Indoor air 26 (2016) 125–137. doi:10.1111/ina.12233.

[50] Z. Zheng, X. Li, J. Pan, X. Luo, A multi-year two-stage stochastic programming model for optimal design and operation of residential photovoltaic-battery systems, Energy and Buildings 239 (2021) 110835. doi:10.1016/j.enbuild.2021.110835.

[51] B. V. Mbuwir, K. Paridari, F. Spiessens, L. Nordström, G. Deconinck, Transfer learning for operational planning of batteries in commercial buildings, in: 2020 IEEE International Conference on Communications, Control, and Computing Technologies for Smart Grids (SmartGridComm), IEEE, 2020, pp. 1–6. doi:10.1109/SmartGridComm47815.2020.9303016.

[52] Y. Peng, Y. Lei, Z. D. Tekler, N. Antanuri, S.-K. Lau, A. Chong, Hybrid system controls of natural ventilation and hvac in mixed-mode buildings: A comprehensive review, Energy and Buildings (2022) 112509. doi:10.1016/j.enbuild.2022.112509.